Resubmitted to Surface & Coatings Technology, September 2020

Path to Single-Crystalline Repair and Manufacture of Ni-based Superalloy using Directional Annealing

T Kalfhaus[†], H Schaar[¶], F Thaler[†], B Ruttert[#], D Sebold[†], J Frenzel[#], I Steinbach[¶], W Theisen[#], O Guillon[†€], TW Clyne[§] & R Vassen[†]*

[†] Forschungszentrum Jülich GmbH
52425 Jülich
Germany

[#] Institut für Werkstoffe
Ruhr-Universität Bochum
44801 Bochum
Germany

[¶] ICAMS
Ruhr-Universität Bochum
44801 Bochum
Germany

[€] Jülich Aachen Research Alliance: JARA-Energy
Forschungszentrum Jülich GmbH
52425 Jülich
Germany

[§] Department of Materials Science & Metallurgy
Cambridge University
27 Charles Babbage Road
Cambridge CB3 0FS, UK

Abstract

Advanced methods for the repair of single-crystalline (SX) Ni-based superalloys are of special interest for the gas turbine industry. Polycrystalline repair approaches show promising results, while the repair of SX materials is still challenging. Directional annealing experiments resulted in large columnar grains by imposing thermal gradients at the abnormal grain growth temperature of a specific Ni-based superalloy. A numerical model of the Bridgman process is applied to provide an insight into the temperature evolution during zone annealing of the Vacuum-Plasma-Spray (VPS) repair coatings with the aim of promoting grain growth from the SX substrate. The results presented here suggest that this is a promising approach to repair or manufacture SX turbine blades.

**Corresponding author: Tel: 0049 2418092758 e-mail: helge.schaar@rub.de

1. Introduction

The outstanding high temperature properties of single-crystalline (SX) Ni-based superalloys result on the one hand from the nature of the γ/γ'-microstructure and on the other hand from the absence of grain boundaries [1-3]. These alloys are widely used to manufacture gas turbine blades for aircrafts and power generating systems. Based on the expensiveness of the components, repair and manufacturing procedures with the potential to reduce the overall costs are of significant interest. Techniques such as laser additive forming [4-8], selective electron beam melting (SEBM) [9] and thermal spraying [10-15] facilitate the production of dense, polycrystalline (PX) crack-free depositions. In addition, scientific work has been carried out with the aim of reconstructing the SX microstructure of worn SX materials. As reported in [9, 16] the additive manufacturing (SEBM) of SX materials results in a SX core surrounded by a PX margin. Laser deposition techniques require a well-defined melt pool and boundary conditions to achieve the requested microstructures, in addition complex geometries complicate the processing [8, 17]. Crystal defects such as stray grains [18-20] and hot cracking [21, 22] can occur, especially in thick deposits.

Recent work on Vacuum-Plasma-Spray (VPS) repair coatings on SX substrates revealed epitaxial regions in the deposited coatings. In that context heat-treatments combined with hot isostatic pressing (HIP) and subsequent rapid quenching [23-25] have been performed to minimize porosity and to promote grain growth. The resulting coatings were dense and epitaxial regions were observed [15]. These results highlight the need for a method that promotes growth of the underling SX material through a PX deposition or outer PX margin.

Directional annealing (or directional recrystallization) is a suitable approach to produce columnar structures or small-scale single crystals by using the motion of a hot zone along the length of the specimen [26-28]. A very fine grain structure and/or prior plastic deformation is necessary for applying this process. The driving force for the columnar growth is the minimization of the grain boundary energy, and presumably the reduction of the dislocation density. In previous investigations abnormal grain growth (AGG) was observed for Ni-based superalloys for temperatures slightly above γ'-solvus, whereas the grain growth beneath the γ'-solvus temperature was suppressed [29-31]. Cox et al. [31] observed a significant influence of the temperature on the recrystallized area for CMSX-4 after indentation in a temperature range between 1565 K and 1574 K.

2. Experimental

In the present study the AGG behavior and the potential of the directional annealing of VPS sprayed CMSX-4 which originates in the SX substrate is investigated. Therefore a 1 mm thick CMSX-4 VPS-repair coating was sprayed onto an SX CMSX-4 substrate. All relevant process parameters are available in literature [15]. In order to minimize the level of porosity and consequently to improve the mechanical properties, the sample was HIP-heat-treated for two hours under a pressure of 150 MPa and at a temperature of 1548 K. Hence the process temperature is slightly below the γ'-solvus temperature of CMSX-4 (taken from [25], 1558 K). A description of the applied experimental setup can be found elsewhere [15, 23, 32].

The sample was cut into six pieces to perform the AGG studies and the directional annealing experiments. Information of the production parameters of sample A8 (HIP) can be found in [15]. This sample is included in the investigation to clarify the influence of the VPS-coating on the microstructure at the standard solution annealing temperature of 1588 K. Sample E1 (Table 1) represents the microstructure after the integrated HIP-heat-treatment process. To be able to precisely evaluate the temperature region above the γ'-solvus temperature, four different samples (E2-E5) were annealed for 0.5 hours at temperatures between 1565 K and 1574 K in a Lenton USF 15/5 (Hope, UK) furnace with a Eurotherm 3204 controller (Worthing, UK). The corresponding processing parameters are given in Table 1. The electron backscatter diffraction (EBSD) technique is used to analyse the grain orientations of the different samples which show AGG by using a ZeissUltra 55 FEG-SEM (Oberkochem; Germany). The EBSD characterization was performed using an accelerating voltage of 15 kV and a step size of 2.6 µm. The step size is chosen in respect of the analysis of large columnar grains which are of particular interest in this work. The software INCA Crystal by Oxford Instruments (Abingdon; United Kingdom) is used for the data analysis of the EBSD mappings to identify the grain size distribution of more than 2000 grains per sample and to exclude the twin grain boundaries (Σ=3) from the analysis. A plot of the grain area over the grain size (calculated equivalent circle diameter (ECD) on the basis of the average grain area) was used to identify the grain size distribution. In the present study, due to the resolution in view of large grains, small grains are not analysed adequately.

For the directional annealing experiment, a thermal gradient was applied to promote directional growth within the PX coating. As a result of the temperature difference between the hot and cold part of the furnace (operated in an Ar/H_2-atmosphere) noticeable thermal gradients develop. The temperatures in the transition zone of the furnace were measured, as can be seen from Fig.1(a) a temperature difference of about 500 K is observed over a length of 280 mm. The PX part of the VPS-sample was put into contact with a CMSX-4 rod (length of 165 mm) whereby the contacting surfaces are both mirror-polished as shown in Fig.1(b). Only the facing surfaces were unprotected to promote the conductive heat-transfer to the cold part of the setup. After heating the tube furnace to a maximum temperature of 1773 K, the setup (including an insulated heat conductor with an attached repair coating on a SX substrate) was pushed to the first position inside the tube furnace. The four positions shown in Fig.1(c) were estimated from the thermal profile (Fig.1(a)) and exhibit temperature values of 1573 K, 1583 K, 1593 K and 1603 K. To facilitate hot zone movement, the front SX part of the setup is kept at each of these positions for two hours to initiate directional grain growth in the SX part, which subsequently grows through the PX coating. The sample was afterwards examined using scanning electron microscopy (SEM) and EBSD.

In the present study aims to assess whether the envisaged repair treatment can be performed in a conventional Bridgman furnace. The thermal field evolution within the furnace during processing was simulated using the commercial FEM-package WinCast. Based on the simulation results the hot zone velocity and the thermal gradient along the growth direction can be evaluated. The numerical model was carried out as described elsewhere [33, 34] in detail. The applied simulations reference the in-house vertical Bridgman-furnace, in the model description radiative and conductive heat transfer processes are considered. Fig.2 shows the geometry of the FEM-model, the different color codes of the heaters indicate that these can be regulated separately. To ensure computational accuracy, a fine mesh consisting of 900,000 polygons respectively 500,000 nodes is used. The required thermo-physical input parameters (thermal conductivity, etc.) were taken from an in-house database as documented in [33, 34] and from literature.

Fig.3(a) shows a SEM image of the microstructure from sample E1 after a HIP-heat-treatment below the γ'-solvus temperature (1548 K). Some porosity is still apparent, although at a relatively low level. Minor oxidation events during spraying result in alumina contamination within the coating as can be seen by the small spherical dark inclusions [15]. The γ/γ'-volume fraction was decreased by using temperatures close to γ'-solvus, the sample is preserved in the solid solution region due to the rapid quenching. Cox et al. [31] presented results where the γ/γ'-volume fraction decreases as the temperature approaches γ'-solvus. Residual γ' particles are known [29, 35] to suppress further grain growth by pinning of the grain boundaries. This can be concluded from Fig. 3(b) where the γ'-particles highlighted by the red arrows hinder further grain growth. The grain size increased to an average ECD of about 5 µm.

3. Results and Discussion

The grain size distribution of sample A8 (HIP) and E1-E5 are presented in Fig.4. The sample A8 (HIP) was chosen due to its low oxygen contamination and its initial grain size [15]. The corresponding grain size distribution relates to a regular heat-treatment, therefore normal grain growth can be assumed [29]. The grain size distribution in Fig.4(a) shows an ECD below 40 µm for more than 75% of the grains. The annealing times of samples E1 and A8 (HIP) were identical (2 hours). The annealing temperature of E1 is 40 K below the solution annealing temperature of 1588 K as applied for A8 (HIP). The remaining γ'-particles hinder the motion of the grain boundaries respectively the grain growth (see Fig.3) which results in a grain size distribution with most grains below 15 µm (Fig.4(b)).

Figs.4(c)-(f) show varying grain size distributions (E2-E5) as the annealing temperature is progressively raised above *γ*'-solvus (1565-1574 K) whereby the annealing time is kept constant (0.5 hours). For the advanced temperatures grains start to appear that are larger than those in the samples A8 (HIP) and E1. All grain size distributions presented in Fig.4 show similar characteristics, the grain size area continuously decreases to an ECD of about 80 µm. There are almost no grains between 80 and 100 µm. All samples show several grain sizes in the range between 100 µm and 160 µm. These bimodal grain size distributions with large grains after short annealing times are typical outcomes of AGG [29]. No effect of temperature can be observed between 1565 K and 1574 K, which is in contrast to the work of Cox et al. [31]. The increase in the recrystallized area might be a consequence of the prior deformation by indentation as performed in the work of Cox et al. and therefore results in a smaller starting grain size.

The reason for AGG is still controversy up to the present day, Abbruzzese et. al found strong evidence for the effect of the texture on AGG in context of rolled materials [46, 47]. In addition to that experimental results by Gladman [48] indicate an influence of the particles within the microstructure on the AGG. For longer annealing times the particles dissolve respectively coarsen, as a consequence locally grains can grow freely which lead to AGG. More recently Lee et al. [49] reported a correlation of faceted grain boundaries and the occurrence of AGG. In respect of the scope of this work and the according experimental analysis, a distinct explanation for the mechanism(s) initiating the AGG cannot be derived. With regard to the presence of the γ'-particles and the temperatures applied in this work, the local dissolution or coarsening of the particles and a resulting AGG seems reasonable.

In respect of the columnar morphology during grain growth, the particle dissolution is a prerequisite whereas the particle dissolution as well as the particle coarsening does not directly initiate the columnar grain formation as reported by Yang and Baker [50].

Fig.5(a)-(c) shows microstructures from sample E6, the SEM micrograph in part a reveals a columnar grain structure with a grain size of several hundred µm. This grain morphology can only be observed at the interface between the PX sample and the SX heat conductor. Directional grain growth which originates in the SX substrate could not be observed. The temperature of the first position was presumable this high that the hot zone velocity was faster than the maximum grain growth velocity. Therefore, the region between the columnar grains and the interface between the PX coating and the SX substrate exhibits a coarse, equiaxed grain structure with a size around 80 µm. The upper region of the sample was in the hot part of the furnace. Fig.5(b) shows an EBSD map of the microstructure from Fig.5(a) whereby a number of twins and twin boundaries are visible. Fig.5(c) shows the grain structure after removing these twins and twin boundaries (Σ=3). Comparing Fig.5(b) and (c) reveals the large number of twin grain boundaries present at the interface of the SX heat conductor and the PX repair coating which indicates a low hot zone velocity. The varying hot zone velocities within the repair coating are a result of the discontinuous movement into the hot zone of the furnace during processing. As reported in literature, the twin boundaries per unit area decrease for increasing hot zone velocities [27], [41]. The large grain (red color in Fig.5(c)) which is orientated in the <001>- direction has a length of more than 400 µm and an average width of about 100 µm (area ~ 43,000 µm^2)

The maximum grain boundary velocity during annealing can be estimated using Eqn.(1).

$$V = \delta \nu \exp\left(\frac{-Q}{\mathrm{RT}}\right)\left\{1 - \exp\left(\frac{-\Delta G}{\mathrm{RT}}\right)\right\} \text{ [36]} \qquad (1)$$

Where Q is the activation energy for the transfer of atoms across the boundary, R is the gas constant, δ is the jump distance (taken from [37], 0.2034 nm) and υ is the atomic jump frequency across the boundary (taken from [38], 10^{13} s^{-1}). The value of Q is implemented in respect of boundary diffusion, hence the energy is approximated as half of the Ni self-diffusion activation energy which is 142.3 kJ mol^{-1} [36]. The effective driving force for recrystallization is ΔG which is independent of the zone annealing speed. ΔG is equal to the change of the stored energy of the grain boundaries

(ΔG_S) whereby it decreases due to the (Zener) particle pinning effect (ΔG_P) as can be seen from Eqn.(2).

$$\Delta G = \Delta G_S - \Delta G_P \text{ [39]} \quad (2)$$

The value of ΔG_S can be approximated by

$$\Delta G_S = \frac{2\gamma}{r_g} \text{ [26, 40-42]} \quad (3)$$

where γ is the (high angle) grain boundary energy (taken from [41], 0.88 J m^{-2}) and r_g is the equivalent radius of the primary recrystallized grains. Due to the pinning effect of the γ'-particles an average initial grain size of 5 µm can be approximated (after the HIP-heat-treatment at 1548 K). The Zener pinning energy is a function of the interfacial energy of the particle, the volume fraction and the radius of the oxide particles [43]. In the present study the contribution of the oxides is neglected in the calculation because of the very small oxide volume fraction [15]. The local occurrence of the oxides makes an approximation difficult in comparison to an ODS superalloy. Nevertheless, with respect to Eqn.(2) the oxides in the coating will decrease ΔG and therefore influence the grain boundary velocity. The resulting stored energy (ΔG) of 704 kJ m^{-3} can be converted by using the density (8,700 kg m^{-3}) and the average molar mass of CMSX-4 (76.08 g mol^{-1}) to a value of 6.16 J mol^{-1}. Applying this value in Eqn.(1) results in a grain boundary velocity for the VPS-sample E1 of about 1 mm min^{-1}.

Directional annealing and AGG are driven by the minimization of the energy of the grain boundaries which increases for decreasing grain sizes (Eqn.(3)). It can be assumed that a HIP-heat-treatment of several minutes should be sufficient to eliminate the "as manufactured" porosity. This results in a dense, fine-grained microstructure with an average grain size below 5 µm. For a reasonable grain size of 1.5 µm and the resulting increased amount of grain-boundary energy, the maximum grain boundary velocity would increase to a value of approximately 4.5 mm min^{-1}. In that context additionally the misorientation between the adjacent grains affects the grain boundary energy.

In Fig.6 the misorientation between the adjacent columnar grains, as can be seen in the microstructure in Fig. 5(a), is illustrated. The corresponding frequency distribution of the measured misorientations is presented in Fig. 7 whereby the distribution is in accordance with experimental results reported by Ukai et al. [45]. Most parts of the frequency distribution of the misorientation is in the high-angle range between 30° to 60° as can be concluded from Fig. 7. This results in relatively large grain boundary interfacial energies and therefore sufficiently high grain boundary mobilities.

In Fig.8 on the left-hand side the simulated temperature distribution within a VPS-sample is illustrated which is heat treated for 1500s. It can be seen that the upper part of the sample reaches the γ'-solvus temperature of 1558 K as intended (the blue line in Fig.8 represents the γ'-solvus isotherm). The temperature distribution in Fig.8 can be fitted by a linear function to determine the thermal gradient within in the sample. The corresponding thermal gradient is about 10 K mm^{-1}, which is presumably sufficient for promoting directional grain growth. In [35] it is reported that successful directional annealing was achieved in context of the Superalloy MA 6000E (γ'-volume fraction of 50%) for a thermal gradient of 5 K mm^{-1}. High γ'-volume fractions will suppress the motion of the grain boundaries for temperatures below γ'-solvus, therefore the grain growth in front of the hot zone is pinned. The thermal gradient is not a critical parameter for CMSX-4 which exhibits a γ'-volume fraction of approximately 85%. Based on this high-volume fraction it can be assumed that even for small thermal gradients a sufficient amount of γ'-particles exists to hinder grain growth. For ODS-alloys with low γ'-volume fractions high thermal gradients are crucial to prevent grain growth ahead of the hot zone as reported in [26].

On the right-hand side of Fig.8 the temperature distribution after 2500s of processing is shown. The hot zone moves about 7 mm along the growth path for a time of 1000s which results in a hot zone velocity of 0.42 mm min^{-1}. As consequence the calculated maximum grain growth velocity is limited to 1mm min^{-1} [44]. The numerical model applied in the present work was successfully validated in advance by comparison to experimental results as reported in [34]. In this context further work is required to facilitate the comparison of the simulation and the experimental results for the processing applied in the present work.

4. Conclusion

In summary, the present work has demonstrated that using a zone annealing methodology on densified VPS-repair coatings (for SX Ni-based superalloys) does offer some promise. The directional annealing experiment resulted in a columnar structure with large grains. AGG occurred for CMSX-4 at temperatures slightly above the γ'-solvus. Calculated grain boundary velocities for these samples are of the order of several mm min^{-1}. This would be a satisfactory magnitude in technical terms. The FEM simulation results of the thermal field evolution within the Bridgman furnace indicate a hot zone movement rate of 0.42 mm min^{-1} for a distance of 7 mm. Such conditions seem to be adequate to allow hot zone movement through a thick polycrystalline VPS-repair coating. In view of producing single crystal repair coatings which are epitaxial with the substrate further investigations are required.

Acknowledgements

The authors acknowledge funding from the Deutsche Forschungsgemeinschaft (DFG), via projects T4, T6 (leading project), B7 and C5 of the collaborative research centre SFB/Transregio 103 'From Atoms to Turbine Blades'. Furthermore, the authors would like to thank Julia Pürstl (Cambridge University) for assistance with the SEM investigations, Stefan Witsch for the EBSD analysis (graphical abstract) and the RWP GmbH for supporting the FEM-Simulations. Funding has also been received from the Leverhulme Trust (ref IN-2016-004), via a grant supporting the Leverhulme International Network on Composites for Extreme Temperatures (LINCET). This supported collaborative work carried out jointly between Cambridge University and FZJ, particularly involving TK, TWC & RV.

References

1. Goldschmidt, D, *Single-Crystal Blades for Gas-Turbines .1. Casting Process and Microstructure.* Materialwissenschaft Und Werkstofftechnik, 1994. **25**(8): p. 311-320.
2. Pollock, TM and S Tin, *Nickel-Based Superalloys for Advanced Turbine Engines: Chemistry, Microstructure, and Properties.* Journal of Propulsion and Power, 2006. **22**(2): p. 361-374.
3. Reed, RC, T Tao, and N Warnken, *Alloys-by-Design: Application to Nickel-Based Single Crystal Superalloys.* Acta Materialia, 2009. **57**(19): p. 5898-5913.
4. Gaumann, M, C Bezencon, P Canalis, and W Kurz, *Single-Crystal Laser Deposition of Superalloys: Processing-Microstructure Maps.* Acta Materialia, 2001. **49**(6): p. 1051-1062.
5. Vilar, R and A Almeida, *Repair and Manufacturing of Single Crystal Ni-Based Superalloys Components by Laser Powder Deposition-a Review.* Journal of Laser Applications, 2015. **27**.
6. Acharya, R and S Das, *Additive Manufacturing of IN 100 Superalloy through Scanning Laser Epitaxy for Turbine Engine Hot-Section Component Repair: Process Development, Modeling, Microstructural Characterization, and Process Control.* Metallurgical and Materials Transactions A-Physical Metallurgy and Materials Science, 2015. **46A**(9): p. 3864-3875.
7. Liu, ZY, H Qi, and L Jiang, *Control of Crystal Orientation and Continuous Growth through Inclination of Coaxial Nozzle in Laser Powder Deposition of Single-Crystal Superalloy.* Journal of Materials Processing Technology, 2016. **230**: p. 177-186.
8. Kaierle, S, L Overmeyer, I Alfred, B Rottwinkel, J Hermsdorf, V Wesling, and N Weidlich, *Single-Crystal Turbine Blade Tip Repair by Laser Cladding and Remelting.* Cirp Journal of Manufacturing Science and Technology, 2017. **19**: p. 196-199.
9. Ramsperger, M, RF Singer, and C Korner, *Microstructure of the Nickel-Base Superalloy Cmsx-4 Fabricated by Selective Electron Beam Melting.* Metallurgical and Materials Transactions A-Physical Metallurgy and Materials Science, 2016. **47A**(3): p. 1469-1480.
10. Okazaki, M, I Ohtera, and Y Harada, *Damage Repair in Cmsx-4 Alloy without Fatigue Life Reduction Penalty.* Metallurgical and Materials Transactions A-Physical Metallurgy and Materials Science, 2004. **35A**(2): p. 535-542.
11. Raoelison, RN, C Verdy, and H Liao, *Cold Gas Dynamic Spray Additive Manufacturing Today: Deposit Possibilities, Technological Solutions and Viable Applications.* Materials & Design, 2017. **133**: p. 266-287.
12. Singh, R, S Schruefer, S Wilson, J Gibmeier, and R Vassen, *Influence of Coating Thickness on Residual Stress and Adhesion-Strength of Cold-Sprayed Inconel 718 Coatings.* Surface & Coatings Technology, 2018. **350**: p. 64-73.
13. Campbell, JE, T Kalfhaus, R Vassen, RP Thompson, J Dean, and TW Clyne, *Mechanical Properties of Sprayed Overlayers on Superalloy Substrates, Obtained Via Indentation Testing.* Acta Materialia, 2018. **154**: p. 237-245.
14. Sun, W, AWY Tan, A Bhowmik, I Marinescu, X Song, W Zhai, F Li, and EJ Liu, *Deposition Characteristics of Cold Sprayed Inconel 718 Particles on Inconel 718 Substrates with Different Surface Conditions.* Materials Science and Engineering a-Structural Materials Properties Microstructure and Processing, 2018. **720**: p. 75-84.
15. Kalfhaus, T, M Schneider, B Ruttert, D Sebold, T Hammerschmidt, J Frenzel, R Drautz, W Theisen, G Eggeler, O Guillon, and R Vassen, *Repair of Ni-Based Single-Crystal Superalloys Using Vacuum Plasma Spray.* Materials & Design, 2019. **168**.
16. Korner, C, M Ramsperger, C Meid, D Burger, P Wollgramm, M Bartsch, and G Eggeler, *Microstructure and Mechanical Properties of Cmsx-4 Single Crystals Prepared by Additive Manufacturing.* Metallurgical and Materials Transactions A-Physical Metallurgy and Materials Science, 2018. **49A**(9): p. 3781-3792.
17. Rottwinkel, B, A Pereira, I Alfred, C Noelke, V Wesling, and S Kaierle, *Turbine Blade Tip Single Crystalline Clad Deposition with Applied Remelting Passes for Well Oriented Volume Extension.* Journal of Laser Applications, 2017. **29**(2).
18. Park, JW, SS Babu, JM Vitek, EA Kenik, and SA David, *Stray Grain Formation in Single Crystal Ni-Base Superalloy Welds.* Journal of Applied Physics, 2003. **94**(6): p. 4203-4209.
19. Anderson, TD, JN DuPont, and T DebRoy, *Origin of Stray Grain Formation in Single-Crystal Superalloy Weld Pools from Heat Transfer and Fluid Flow Modeling.* Acta Materialia, 2010. **58**(4): p. 1441-1454.
20. Anderson, TD, JN Dupont, and T Debroy, *Stray Grain Formation in Welds of Single-Crystal Ni-Base Superalloy Cmsx-4.* Metallurgical and Materials Transactions A-Physical Metallurgy and Materials Science, 2010. **41A**(1): p. 181-193.

21. *Ebrahimnia, M, FM Ghaini, and HR Shahverdi, Hot Cracking in Pulsed Laser Processing of a Nickel Based Superalloy Built up by Electrospark Deposition. Science and Technology of Welding and Joining, 2014.* ***19****(1): p. 25-29.*
22. *Rong, P, N Wang, L Wang, RN Yang, and WJ Yao, The Influence of Grain Boundary Angle on the Hot Cracking of Single Crystal Superalloy Dd6. Journal of Alloys and Compounds, 2016.* ***676****: p. 181-186.*
23. *Ruttert, B, M Ramsperger, LM Roncery, I Lopez-Galilea, C Korner, and W Theisen, Impact of Hot Isostatic Pressing on Microstructures of CMSX-4 Ni-Base Superalloy Fabricated by Selective Electron Beam Melting. Materials & Design, 2016.* ***110****: p. 720-727.*
24. *Roncery, LM, I Lopez-Galilea, B Ruttert, D Burger, P Wollgramm, G Eggeler, and W Theisen, On the Effect of Hot Isostatic Pressing on the Creep Life of a Single Crystal Superalloys. Advanced Engineering Materials, 2016.* ***18****(8): p. 1381-1387.*
25. *Roncery, LM, I Lopez-Galilea, B Ruttert, S Huth, and W Theisen, Influence of Temperature, Pressure, and Cooling Rate During Hot Isostatic Pressing on the Microstructure of an SX Ni-Base Superalloy. Materials & Design, 2016.* ***97****: p. 544-552.*
26. *Li, J, SL Johns, BM Iliescu, HJ Frost, and I Baker, The Effect of Hot Zone Velocity and Temperature Gradient on the Directional Recrystallization of Polycrystalline Nickel. Acta Materialia, 2002.* ***50****(18): p. 4491-4497.*
27. *Baker, I, B Iliescu, J Li, and HJ Frost, Experiments and Simulations of Directionally Annealed ODS MA 754. Materials Science and Engineering a-Structural Materials Properties Microstructure and Processing, 2008.* ***492****(1-2): p. 353-363.*
28. *Ukai, S, K Taya, K Nakamura, MS Aghamiri, N Oono, S Hayashi, and T Okuda, Directional Recrystallization by Zone Annealing in a Ni-Base ODS Superalloy. Journal of Alloys and Compounds, 2018.* ***744****: p. 204-210.*
29. *Lee, SB, DY Yoon, and MF Henry, Abnormal Grain Growth and Grain Boundary Faceting in a Model Ni-Base Superalloy. Acta Materialia, 2000.* ***48****(12): p. 3071-3080.*
30. *Cho, YK, DY Yoon, and MF Henry, The Effect of Deformation and Pre-Heat-Treatment on Abnormal Grain Growth in Rene 88 Superalloy. Metallurgical and Materials Transactions A-Physical Metallurgy and Materials Science, 2001.* ***32****(12): p. 3077-3090.*
31. *Cox, DC, B Roebuck, CMF Rae, and RC Reed, Recrystallisation of Single Crystal Superalloy Cmsx-4. Materials Science and Technology, 2003.* ***19****(4): p. 440-446.*
32. *Ruttert, B, D Burger, LM Roncery, AB Parsa, P Wollgramm, G Eggeler, and W Theisen, Rejuvenation of Creep Resistance of a Ni-Base Single-Crystal Superalloy by Hot Isostatic Pressing. Materials & Design, 2017.* ***134****: p. 418-425.*
33. *Hallensleben, P, H Schaar, P Thome, N Jons, A Jafarizadeh, I Steinbach, G Eggeler, and J Frenzel, On the Evolution of Cast Microstructures During Processing of Single Crystal Ni-Base Superalloys Using a Bridgman Seed Technique. Materials & Design, 2017.* ***128****: p. 98-111.*
34. *Hallensleben, P, F Scholz, P Thome, H Schaar, I Steinbach, G Eggeler, and J Frenzel, On Crystal Mosaicity in Single Crystal Ni-Based Superalloys. Crystals, 2019.* ***9****(3).*
35. *Hotzler, RK and TK Glasgow, The Influence of Gamma-' on the Recrystallization of an Oxide Dispersion Strengthened Super-Alloy - Ma-6000e. Metallurgical Transactions A-Physical Metallurgy and Materials Science, 1982.* ***13****(10): p. 1665-1674.*
36. *Christian, JW, The Theory of Transformations in Metals and Alloys : An Advanced Textbook in Physical Metallurgy. 1975: Pergamon.*
37. *Weissmann, S, B Post, ME Morse, and HF McMurdie, Selected Powder Diffraction Data for Metals and Alloys. 1979: International Centre for Diffraction Data.*
38. *Lide, DR, Crc Handbook of Chemistry and Physics : A Ready-Reference Book of Chemical and Physical Data. 2004: CRC Press.*
39. *Sha, W and H Bhadeshia, Directional Recrystallization in Mechanically Alloyed Oxide Dispersion-Strengthened Metals by Annealing in a Moving Temperature-Gradient. Journal of Materials Science, 1995.* ***30****(6): p. 1439-1444.*
40. *Frost, HJ, CV Thompson, and DT Walton, Simulation of Thin-Film Grain Structures .2. Abnormal Grain-Growth. Acta Metallurgica Et Materialia, 1992.* ***40****(4): p. 779-793.*
41. *Carel, R, CV Thompson, and HJ Frost, Computer Simulation of Strain Energy Effects Vs Surface and Interface Energy Effects on Grain Growth in Thin Films. Acta Materialia, 1996.* ***44****(6): p. 2479-2494.*
42. *Li, J and I Baker, An EBSD Study of Directionally Recrystallized Cold-Rolled Nickel. Materials Science and Engineering a-Structural Materials Properties Microstructure and Processing, 2005.* ***392****(1-2): p. 8-22.*

43. *Nishizawa, T, I Ohnuma, and K Ishida, Examination of the Zener Relationship between Grain Size and Particle Dispersion. Materials Transactions Jim, 1997.* ***38****(11): p. 950-956.*
44. *Baloch, MM and H Bhadeshia, Directional Recrystallization in Inconel Ma 6000 Nickel-Base Oxide Dispersion Strengthened Superalloy. Materials Science and Technology, 1990.* ***6****(12): p. 1236-1246.*
45 *S Ukai, K Taya, K Nakamura, MS Aghamiri, N Oono, S. Hayashi and T. Okuda, Directional recrystallization by zone annealing in a Ni-based ODS superalloy, Journal of Alloys and Compounds, 2017.*
46 *G. Abbruzzese and K. Lücke, A Theory of Texture Controlled Grain Growth - I. Derivation and General Discussion", Acta Metall.,1986.34: p. 905 - 34 (1986) 905.*
47 *H. Eichelkraut, G. Abbruzzese and K. Lücke, A Theory of Texture Controlled Grain Growth - II. Numerical and Analytical Treatment of Grain Growth in the Presence of Two Texture Components,* Acta Metall., 1988.36: p. 55-68.
48 *T. Gladman, The theory and inhibition of abnormal grain growth in steels, JOM, 1992.44: p. 21–24*
49 *B. Lee, Y. Yoon, and M.F. Henry, Abnormal grain growth and grain boundary faceting in a model Ni-base superalloy, Acta Mater., 2000.48: p. 3071-3080*
50 *C. Yang and I. Baker, Effect of soluble particles on microstructural evolution during directional recrystallization, Acta Mater., 2020.188: p. 288-301*

Tables

Code	Heat-Treatment
A8 (HIP)	HIP: 2 h 1588 K, 4h 1413 K; Vac: 16 h 1133 K
E1	HIP: 2 h 1548 K
E2	HIP: 2 h 1548 K; Vac: 0,5 h 1565 K
E3	HIP: 2 h 1548 K; Vac: 0,5 h 1568 K
E4	HIP: 2 h 1548 K; Vac: 0,5 h 1571 K
E5	HIP: 2 h 1548 K; Vac: 0,5 h 1574 K
E6	HIP: 2 h 1548 K; directional grain growth exp.

Table I Sample codes and heat-treatment conditions

Figure Captions

Fig.1 *Experimental set-up in order to achieve directional grain growth: (a) Temperature profile of the tube furnace in the transition zone; (b) Cross section of polycrystalline repair coating on single crystal CMSX-4 substrate, with good insulation except for the interface between them (c) Sample in the transition zone of the tube furnace, with four locations indicated where temperature was monitored*

Fig.2 *Geometry of the FEM model of the applied vertical Bridgman furnace, on the right-hand side a magnification of the mesh of the melt feedstock and the crucible is presented*

Fig.3 *SEM micrograph of sample E1 after the HIP-heat-treatment (below γ'-solvus) at 1548 K for 2 hours, at a pressure of 150 MPa, showing (a) decreased γ/γ'-volume fraction and (b) suppression of grain growth by remaining γ'-particles (red arrows)*

Fig.4 *Grain size distribution from more than 2000 grains, obtained using EBSD results for samples: (a) A8 (HIP), (b) E1, (c) E2, (d) E3, (e) E4 and (f) E5*

Fig.5 *Microstructure of sample E6 after directional grain growth SEM: (a) SEM micrograph of backscattered electrons; (b) EBSD quality pattern and (c) EBSD without twin grain boundaries. The inverse pole figure indicates the crystal orientation*

Fig. 6 *Plot of the misorientations between the adjacent grains within the microstructure presented in part a of Fig. 5*

Fig. 7 *Frequency Distribution of the measured misorientations within the microstructure as illustrated in Fig. 6*

Fig.8 *Simulated thermal field evolution for the time steps of 1500s and 2500s in the sample E6 when processed in a vertical Bridgman furnace; the isotherm of the γ'-solvus temperature is superimposed as blue line*

Figures

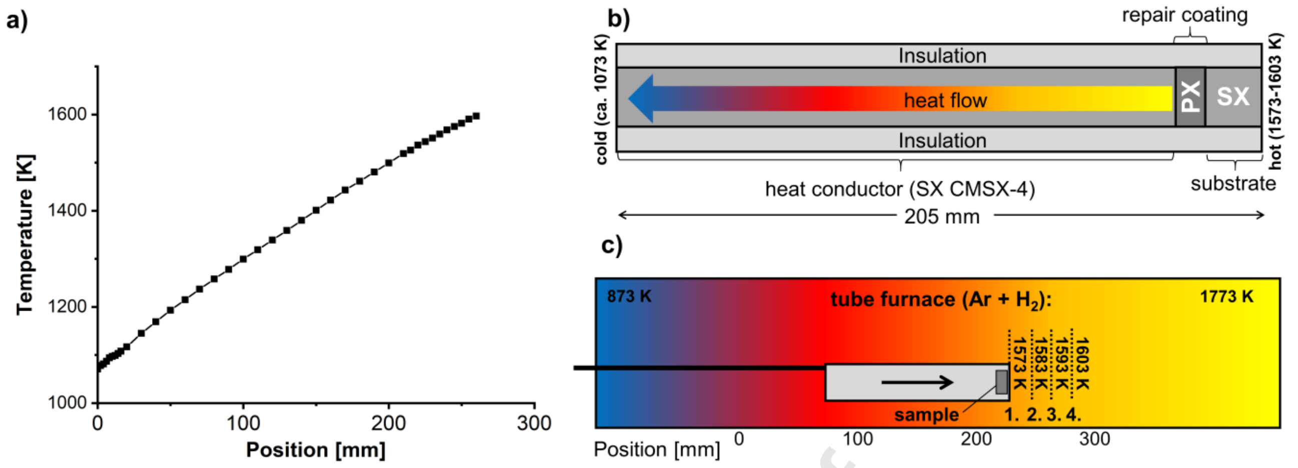

Fig.1 *Experimental setup in order to achieve directional grain growth: (a) Temperature profile of the tube furnace in the transition zone; (b) Cross section of polycrystalline repair coating on single crystal CMSX-4 substrate, with good insulation except for the interface between them (c) Sample in the transition zone of the tube furnace, with four locations indicated where temperature was monitored*

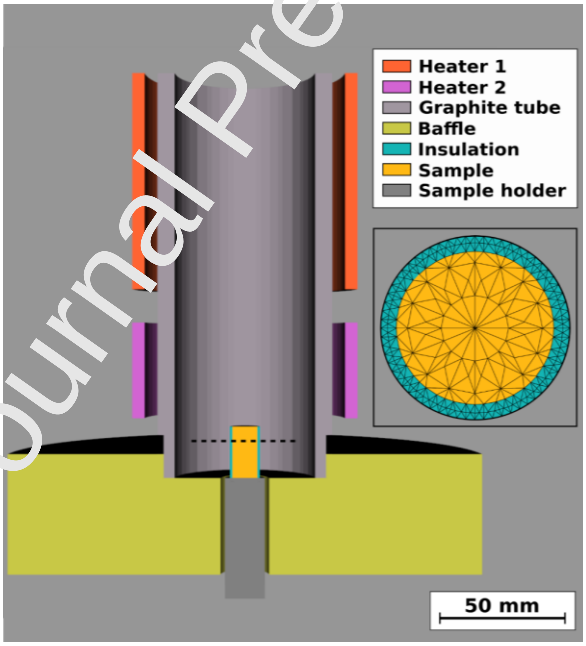

Fig.2 *Geometry of the FEM model of the applied vertical Bridgman furnace, on the right-hand side a magnification of the mesh of the melt feedstock and the crucible is presented*

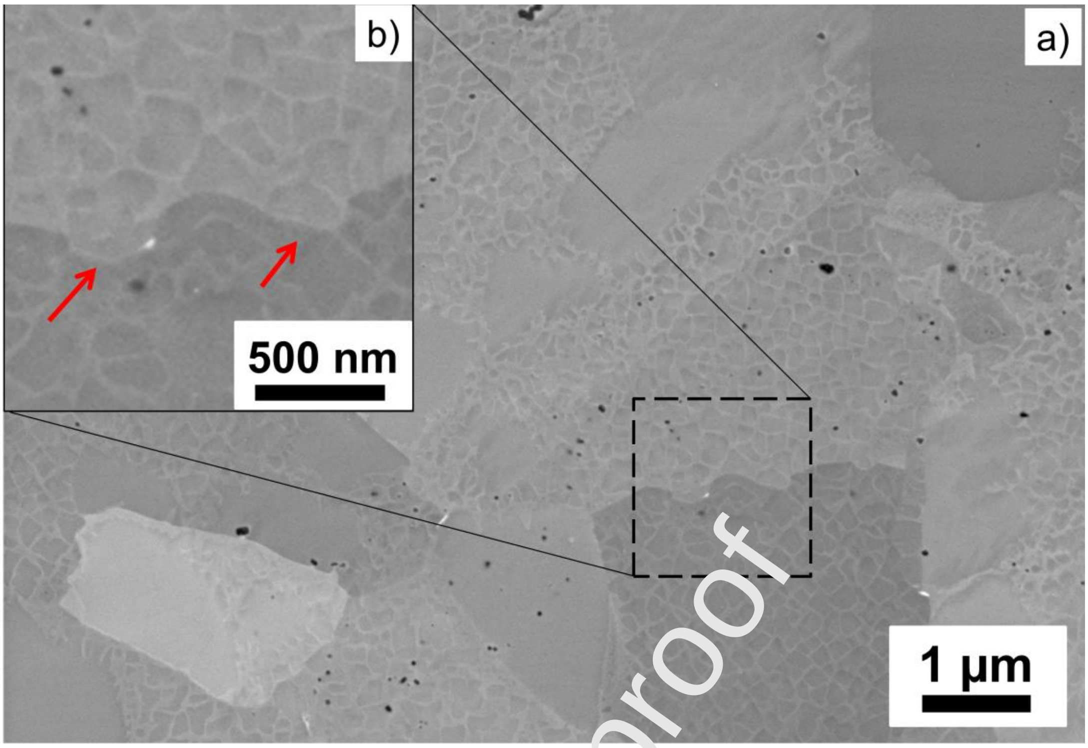

Fig.3 *SEM micrograph of sample E1 after the HIP-heat-treatment (below γ'-solvus) at 1548 K for 2 hours, at a pressure of 150 MPa, showing (a) decreased γ/γ'-volume fraction and (b) suppression of grain growth by remaining γ'-particles (red arrows)*

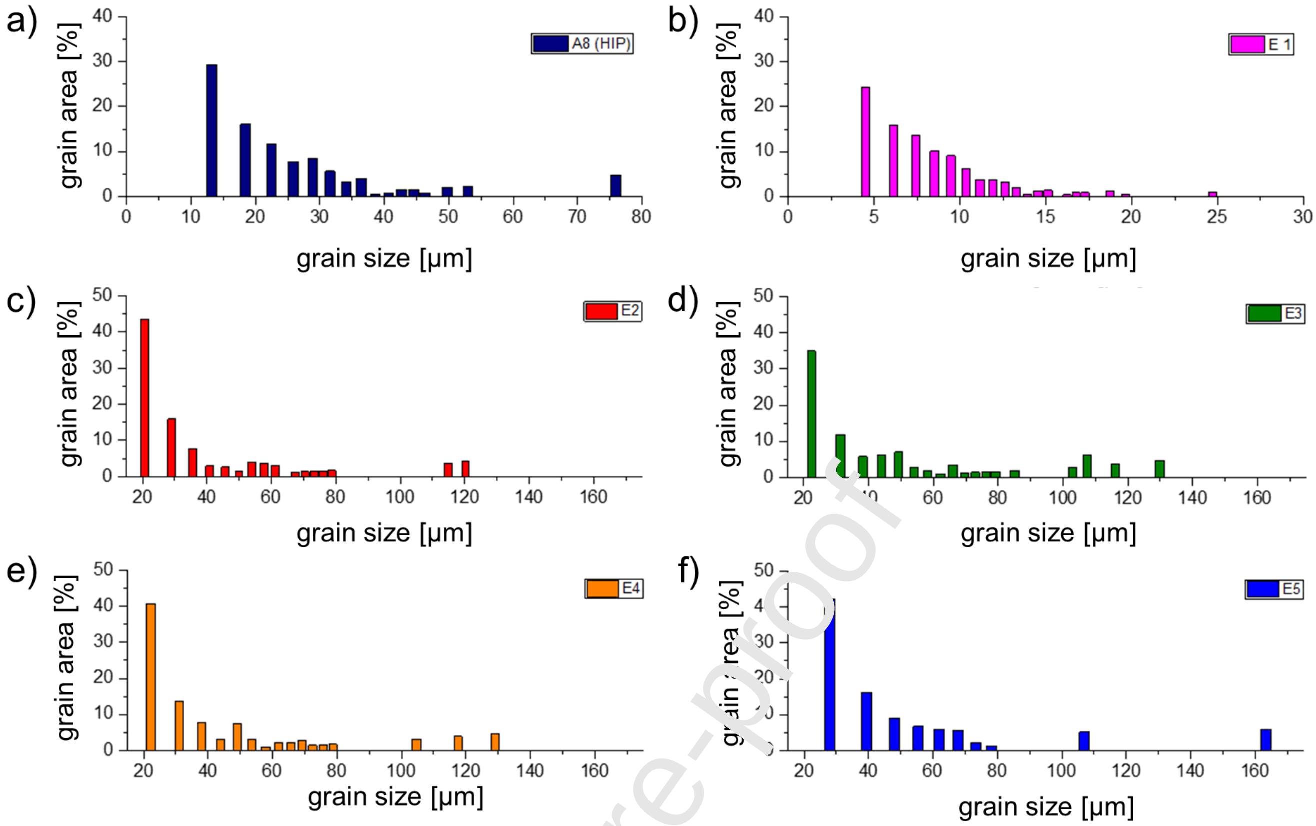

Fig.4 *Grain size distribution from more than 2000 grains, obtained using EBSD results for samples: (a) A8 (HIP), (b) E1, (c) E2, (d) E3, (e) E4 and (f) E5*

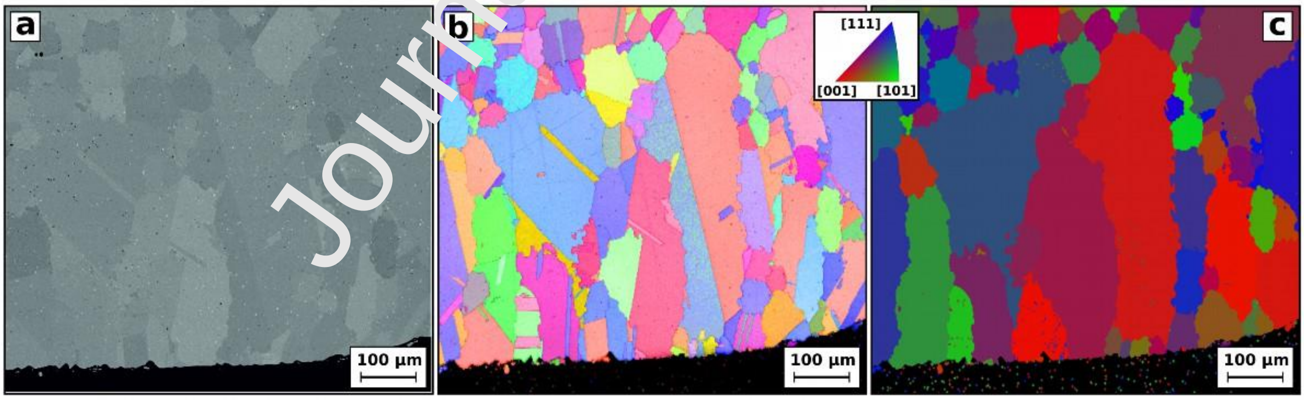

Fig.5 *Microstructure of sample E6 after directional grain growth SEM: (a) SEM micrograph of backscattered electrons; (b) EBSD quality pattern and (c) EBSD without twin grain boundaries. The inverse pole figure indicates the crystal orientation*

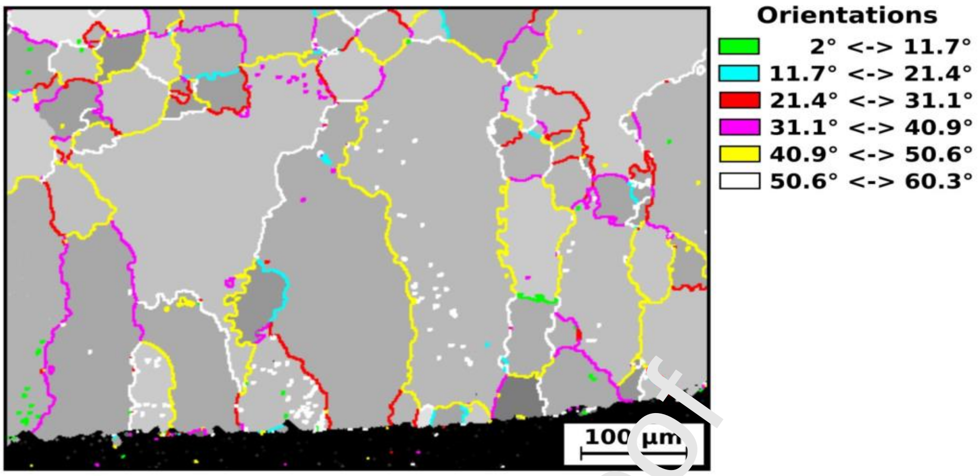

Fig. 6 Plot of the misorientations between the adjacent grains within the microstructure presented in part a of Fig. 5

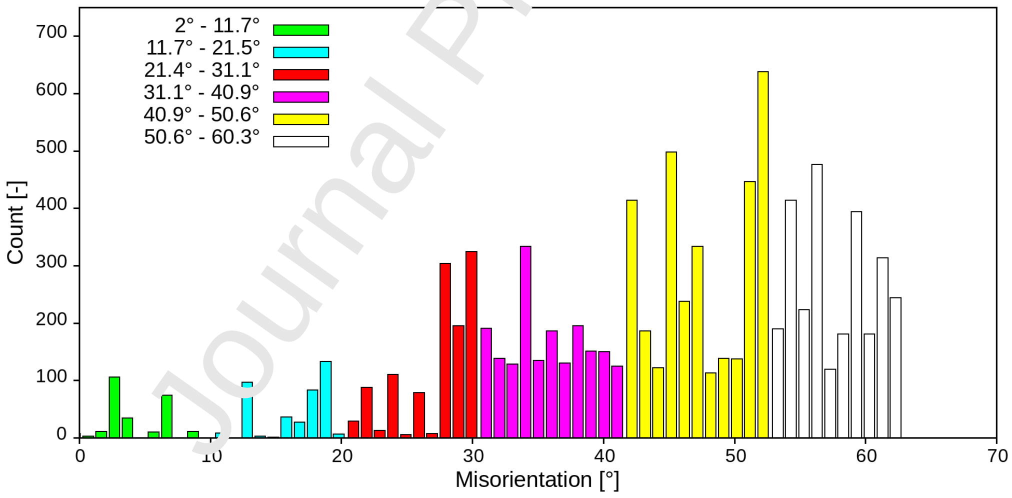

Fig. 7 Frequency Distribution of the measured misorientations within the microstructure as illustrated in Fig. 6

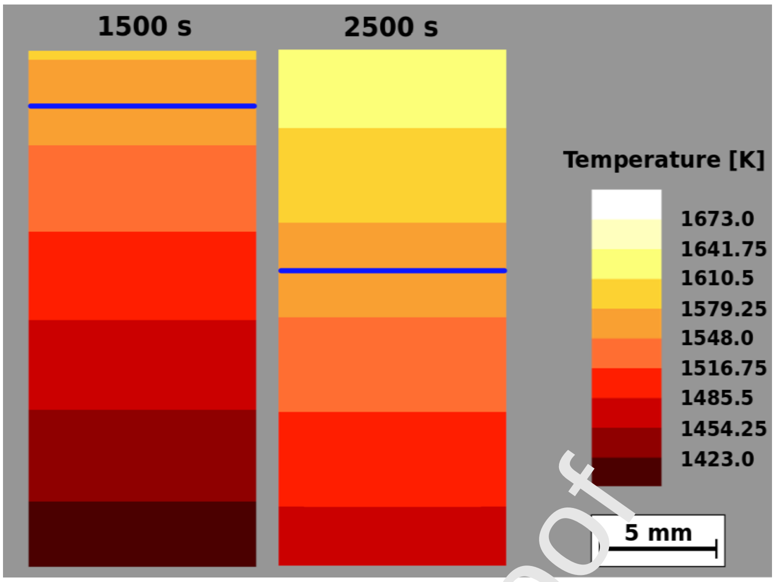

Fig.8 *Simulated thermal field evolution for the time steps of 1500s and 2500s in the sample E6 when processed in a vertical Bridgman furnace; the isotherm of the γ'-solvus temperature is superimposed as blue line*

Credit author statement

T. Kalfhaus: Conceptualization, Investigation, Methodology, Writing - Original Draft, Writing - Review & Editing**, H. Schaar**: Conceptualization, Software, Methodology, Writing - Original Draft, Writing - Review & Editing, **F. Thaler:** Investigation, **B. Ruttert:** Investigation, Writing - Original Draft, Writing - Review & Editing, **D. Sebold:** Investigation, **J. Frenzel:** Writing - Original Draft, Writing - Review & Editing, **I. Steinbach:** Writing - Original Draft, Writing - Review & Editing**, W. Theisen:** Writing - Review & Editing, **O. Guillon:** Writing - Review & Editing, **T.W. Clyne:** Writing - Original Draft, Writing - Review & Editing, **R. Vassen:** Writing - Original Draft, Writing - Review & Editing

Declaration of interests

☒ The authors declare that they have no known competing financial interests or personal relationships that could have appeared to influence the work reported in this paper.

☐The authors declare the following financial interests/personal relationships which may be considered as potential competing interests:

Graphical abstract

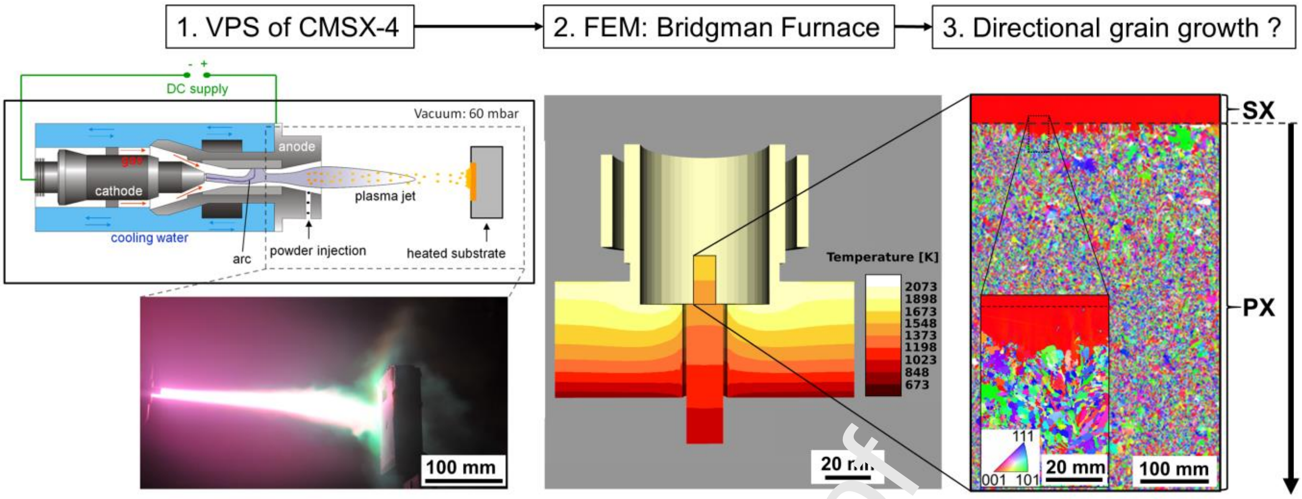

Highlights:

- Abnormal grain growth behavior of vacuum plasma sprayed superalloy coatings
- Directional annealing of fine-grained repair coating results in columnar grains
- FEM simulation of a Bridgeman furnace for directional annealing
- Single Crystalline repair by simulating grain growth from single crystal substrate